

1

2 A new attraction-detachment model for explaining flow  
3 sliding in clay-rich tephtras

4 **Max O. Kluger<sup>1</sup>, Vicki G. Moon<sup>2</sup>, Stefan Kreiter<sup>1</sup>, David J. Lowe<sup>2</sup>, G.J.**

5 **Churchman<sup>3</sup>, Daniel A. Hepp<sup>1</sup>, David Seibel<sup>1</sup>, M. Ehsan Jorat<sup>4</sup>, and Tobias Mörz<sup>1</sup>**

6 <sup>1</sup>*Marum – Center for Marine Environmental Sciences, University of Bremen, Leobener*  
7 *Straße, 28359 Bremen, Germany*

8 <sup>2</sup>*School of Science, University of Waikato, Private Bag 3105, Hamilton 3240, New*  
9 *Zealand*

10 <sup>3</sup>*School of Agriculture, Food and Wine, University of Adelaide, Adelaide 5005, Australia*

11 <sup>4</sup>*School of Science, Engineering and Technology, Abertay University, Dundee, DD11HG,*  
12 *UK*

13

14

15 Final pre-publication version 29 November 2016

16

17 *Final version citation:* Kluger, M.O., Moon, V.G., Kreiter, S., Lowe, D.J., Churchman, G.J.,

18 Hepp, D.A., Seibel, D., Jorat, M.E., Mörz, T. 2017. A new attraction-detachment model for

19 explaining flow sliding in clay-rich tephtras. *Geology* 45, 131-134 (online 8 Dec 2016, DOI:

20 10.1130/G38560.1)

21

22

23

24 **ABSTRACT**

25         Altered pyroclastic (tephra) deposits are highly susceptible to landsliding, leading  
26 to fatalities and property damage every year. Halloysite, a low-activity clay mineral, is  
27 commonly associated with landslide-prone layers within altered tephra successions,  
28 especially in deposits with high sensitivity, which describes the post-failure strength loss.  
29 However, the precise role of halloysite in the development of sensitivity, and thus in  
30 sudden and unpredictable landsliding, is unknown. Here we show that an abundance of  
31 mushroom cap-shaped (MCS) spheroidal halloysite governs the development of  
32 sensitivity, and hence proneness to landsliding, in altered rhyolitic tephra, North Island,  
33 New Zealand. We found that a highly sensitive layer, which was involved in a flow slide,  
34 has a remarkably high content of aggregated MCS spheroids with substantial openings on  
35 one side. We suggest that short-range electrostatic and van der Waals' interactions  
36 enabled the MCS spheroids to form interconnected aggregates by attraction between the  
37 edges of numerous paired silanol and aluminol sheets that are exposed in the openings  
38 and the convex silanol faces on the exterior surfaces of adjacent MCS spheroids. If these  
39 weak attractions are overcome during slope failure, multiple, weakly attracted MCS  
40 spheroids can be separated from one another, and the prevailing repulsion between  
41 exterior MCS surfaces results in a low remolded shear strength, a high sensitivity, and a  
42 high propensity for flow sliding. The evidence indicates that the attraction-detachment  
43 model explains the high sensitivity and contributes to an improved understanding of the  
44 mechanisms of flow sliding in sensitive, altered tephra rich in spheroidal halloysite.

45

46

47 **INTRODUCTION**

48 Most East Asian and western Pacific countries are located in tectonically active,  
49 high-rainfall areas where landslides are a major natural hazard. These landslides are  
50 typically triggered by rainstorms or earthquakes, and are responsible for fatalities and  
51 enormous property damage every year. Many destructive landslides have occurred in  
52 pyroclastic deposits in Japan, Indonesia, Hong Kong, and New Zealand (Chau et al.,  
53 2004; Chigira, 2014; Moon, 2016), such deposits commonly containing layers rich in  
54 clay minerals formed mainly by chemical weathering either during pedogenesis or  
55 diagenesis. In regions with predominantly rhyolitic volcanism, halloysite is a common  
56 clay mineral (Churchman and Lowe, 2012) and is therefore potentially a key geological  
57 factor increasing the risk of landslides (Kirk et al., 1997; Chigira, 2014). Halloysite is a  
58 1:1 Si:Al layered aluminosilicate member of the kaolin subgroup that exhibits various  
59 structural morphologies including tubes, spheroids, polyhedrons, plates and books  
60 (Joussein et al., 2005; Cunningham et al., 2016).

61 Spheroidal halloysite, in particular, has been recognized in landslide-prone layers  
62 of pyroclastic material in Japan (Tanaka, 1992) and New Zealand (Smalley et al., 1980).  
63 Smalley et al. (1980) linked a high content of spheroidal halloysite to high sensitivity.  
64 Sensitivity refers to the post-failure strength loss in the failure zone during landsliding,  
65 and is quantified in the laboratory as the ratio of the undisturbed to remolded undrained  
66 shear strength at the same water content (Terzaghi, 1944). High sensitivities were first  
67 described for post-glacial, brackish and marine clayey sediments in the Northern  
68 Hemisphere (Skempton and Northey, 1952) that are subject to landslides with

69 dimensions and long runout distances difficult to predict. In this study, we investigate  
70 processes that have led to high sensitivity in halloysite-rich pyroclastic materials in order  
71 to improve landslide-hazard evaluation.

72

### 73 **GEOLOGICAL SETTING**

74       Much of the central part of New Zealand's North Island is covered by thick  
75 rhyolitic tephra (Lowe, 2011) derived from eruptions in the Taupo Volcanic Zone  
76 (Briggs et al., 2005), which are commonly altered into halloysite-rich successions. We  
77 focus here on a coastal flow slide at Omokoroa, Bay of Plenty (Fig. 1A), where ~10,000  
78 m<sup>3</sup> of material were transported downslope over long distance into a lagoon in 1979  
79 (Moon et al., 2015) as well as two minor reactivations in 2011 and 2012. The 1979 event  
80 was likely initiated in a white, highly sensitive layer with high spheroidal halloysite  
81 concentration (Smalley et al., 1980) (and lacking any detectable allophane; Cunningham  
82 et al., 2016).

83       We have analyzed a 40-m-long sediment core, Omok-1, which we bored via  
84 rotary flush drilling in unfailed material near the headwall (Fig. 1B). The lithology of  
85 Omok-1 was determined by correlation with units of a previously studied adjacent  
86 headwall face (Moon et al., 2015) comprising a succession mainly of Quaternary rhyolitic  
87 tephra: overlying lignite at the base of the core, the Pahoia Tephra sequence includes the  
88 Te Puna Ignimbrite (ca. 0.93 Ma) and a series of altered tephra which are informally  
89 divided into lower and upper Pahoia Tephra units based on two distinct paleosols (P1 and  
90 P3). All these deposits and paleosols are overlain by successions of younger altered  
91 tephra called Hamilton Ash beds (ca. 0.35 to ca. 0.05 Ma) and late Quaternary tephra (<

92 ca. 0.05 Ma) (Figs. 1C and 2A). The lower Pahoia Tephra include the 0.3-m-thick,  
93 white, highly sensitive clay-rich layer that failed in 1979 (Fig. 1C), having high porosity  
94 and high natural water content (Smalley et al., 1980).

95

## 96 **METHODS**

97 We performed laboratory vane shear tests on samples from the Pahoia Tephra  
98 sequence and Hamilton Ash beds to measure the sensitivity  $S$ :

$$99 \quad S = s_u / s_r \quad (1)$$

100 where the undisturbed strength ( $s_u$ ) was measured on the intact surface of the split core,  
101 and the remolded strength ( $s_r$ ) was measured on core samples with the same water  
102 content but that been kneaded by hand for 10 min (Jacquet, 1990). Halloysite  
103 concentration in bulk samples was measured by X-ray diffraction (XRD) using a Philips  
104 PW analytical diffractometer, and quantification was performed using QUAX software  
105 (Vogt et al., 2002). Scanning electron microscopy (SEM) was undertaken with a Zeiss  
106 Supra40 microscope on 24 shock-frozen, freeze-dried, and gold-coated bulk core samples  
107 (Reed, 2005). The relative abundances of halloysite particles having distinct  
108 morphologies were quantified using a point-counting approach (Frolov and Maling,  
109 1969). Six representative SEM images of planar soil surfaces were chosen for each  
110 sample, and at least 600 particles were counted based on rectangular grids. In the white,  
111 highly sensitive layer, the change of halloysite particle arrangement upon remolding was  
112 quantified by comparing 20 SEM images of undisturbed and remolded material,  
113 providing > 1000 counts respectively. The spheroid diameters were measured from six  
114 representative particles per SEM image.

115 **HIGHLY SENSITIVE SLIDE-PRONE LAYER DOMINATED BY SPHEROIDAL**  
116 **HALLOYSITE**

117 The sensitivity is low in the upper Pahoia Tephra, especially in the paleosols P2  
118 and P3 (Fig. 2A and 2B). However, the sensitivity tends to increase with depth, reaching  
119 values of 15–20 in the lower Pahoia Tephra. The highest sensitivity (Rosenqvist, 1953)  
120 of  $S = 55$ , and the lowest remolded shear strength within the profile of  $s_r = 1.4$  kPa, were  
121 measured in the white, highly sensitive layer at 23 m depth.

122 The upper Pahoia Tephra have a halloysite content of 10–20 wt% comprising  
123 almost entirely tubular halloysite (Figs. 2C and 2D). The lower Pahoia Tephra have  
124 40–50 wt% halloysite comprising mostly spheroidal particles. In the highly sensitive  
125 layer, 76% of the halloysite is spheroidal and the spheroid sizes are greater than those in  
126 the surrounding layers (Figs. 2D and 2E). A three-dimensional line plot reveals a clear  
127 correlation between high sensitivities and high halloysite bulk concentration, and a high  
128 content of spheroids with large diameters (Fig. 2F). The high sensitivity is associated  
129 with low remolded shear strength rather than with high undisturbed shear strength (Fig.  
130 2G).

131 We found that deposits with high tubular halloysite content hamper sensitivity  
132 development, whereas halloysite spheroids facilitate sensitivity and dominate the highly  
133 sensitive layer at 23 m depth within the lower Pahoia Tephra. The highly sensitive layer  
134 has low remolded shear strength consequent after failure, which, together with its high  
135 water content (Smalley et al., 1980), partly contributed to the long runout distance of the  
136 flow slide at Omokoroa.

137

138 **NEW HALLOYSITE MORPHOLOGY**

139         We present here first observations of a previously unreported halloysite particle  
140 morphology, which is visible in the SEM images of the remolded halloysite fabrics of the  
141 highly sensitive layer. In the undisturbed state, the spheroidal halloysites are distinctly  
142 aggregated into networks of well-connected particles (Figs. 3E and 3F). After remolding,  
143 however, most of the aggregates have broken apart into small, loose clusters or individual  
144 halloysite particles that are typically ~250–400 nm in diameter (Figs. 3G and 3H).  
145 Individual spheroids have distinctive “deformities” in the form of openings ~80–160 nm  
146 in diameter on one side. These openings were previously hidden by contact with other  
147 spheroids. The deformities give the particles an ovate “mushroom cap” appearance.  
148 Point-counting individual mushroom-cap shapes in both undisturbed (aggregated) and  
149 remolded (disaggregated) samples showed that the observable mushroom-cap shapes  
150 were much more abundant in the remolded samples, increasing from  $4.4\% \pm 3.2\%$  to  
151  $44.9\% \pm 11.6\%$ .

152

153 **ATTRACTION-DETACHMENT MODEL FOR FLOW SLIDING IN ALTERED**  
154 **TEPHRAS**

155         The open-sided, mushroom cap-shaped halloysite morphology has not been  
156 reported previously. Because this particular morphology overwhelmingly occurs in the  
157 highly sensitive slide-prone layer, we hypothesize that this unique particle shape controls  
158 the mechanical behavior of halloysite clays.

159         Halloysite is composed of an Al-octahedral (aluminol) sheet with a net positive  
160 charge and a Si-tetrahedral (silanol) sheet with a net negative charge at pH values

161 between ~2 and ~8 (Fig. 3I) (Churchman et al., 2016). The two sheets have slightly  
162 different dimensions, with the silanol sheet being larger. This misfit in the sheet sizes  
163 causes the halloysite layer to be curved (Churchman and Lowe, 2012), with the larger  
164 negatively charged silanol sheet on the outside of the curvature and the positively  
165 charged smaller aluminol sheet on the inside. The halloysite spheroids observed in our  
166 study are most likely composed of concentrically stacked 1:1 layers, i.e., with an onion-  
167 like structure, as shown in numerous studies including those on spheroidal halloysite  
168 derived from altered tephra in New Zealand, Japan, and Argentina (Wada et al., 1977;  
169 Kirkman, 1981; Cravero et al., 2012; Berthonneau et al., 2015). For a perfect halloysite  
170 spheroid, the outermost silanol surface carries a net negative charge and hence the  
171 electrostatic interactions between individual spheroids would be repulsive (Fig. 3I). Our  
172 study shows, however, a halloysite structure where both silanol and aluminol layers are  
173 exposed at spheroid openings and therefore charges within the openings would  
174 correspondingly be weakly positive or neutral overall (Fig. 3J), as indicated from charge  
175 density-functional tight-binding modeling applied to halloysite nanotubes (Guimarães et  
176 al., 2010). If sufficient numbers of positively charged openings are exposed, the  
177 electrostatic interactions between them and the negative exterior silanol surfaces would  
178 allow the mushroom cap-shaped spheroids to form stacked aggregates (Fig. 3K). If the  
179 paired silanol and aluminol sheets exposed in the openings are neutral overall, then a net  
180 increase in particle attraction will still occur because electrostatic repulsion is reduced  
181 and the larger contact areas lead to higher van der Waals forces (Israelachvili, 2011).

182         During diagenesis via hydrolysis of volcanic glass (Cunningham et al., 2016), the  
183 halloysite spheroids may form consecutively on top of one another in pore spaces,

184 generating the distinct openings during synthesis. The attractive forces between the  
185 openings and the convex exterior surfaces are demonstrably strong enough to allow for  
186 the formation of aggregates, but also permit easy disaggregation by mechanical  
187 detachment during shear (Fig. 3L). New random contacts between convex silanol  
188 surfaces probably lead to a decrease in average attraction between particles. We posit that  
189 the detachment of attractive spheroidal particle contacts, in the presence of abundant  
190 water having negligible interaction with ions in soil solution because of the inactive  
191 nature of halloysite (Smalley et al., 1980), leads to the very low post-failure shear  
192 strength, facilitating a flow slide with long runout distance. The interparticle attraction-  
193 detachment model appears to successfully explain (at nanoscale dimensions) the post-  
194 failure behavior of the highly sensitive tephra layer at Omokoroa, which is dominated by  
195 the imperfect halloysite spheroids. The question therefore arises whether similar altered  
196 tephra elsewhere have high contents of spheroidal halloysite with potentially hidden  
197 mushroom-cap forms, and if such forms helped mobilize other landslides in the past.

198

## 199 **CONCLUSIONS**

200 We investigated a sequence of altered, rhyolitic Quaternary tephra in New  
201 Zealand and the reasons why a landslide-prone layer dominated by spheroidal halloysite  
202 was highly sensitive. We explain this high sensitivity with an electrostatic attraction-  
203 detachment model. Weakly positive or neutral charges on silanol and aluminol sheet  
204 edges exposed in the concave openings of spheroidal halloysite particles were attracted to  
205 the negatively charged convex silanol surfaces of adjacent spheroids. Such short-range  
206 attractions between spheroid openings, and the exterior surfaces of adjacent spheroids,

207 stabilize an aggregated halloysite framework. If the aggregates are detached by  
208 remolding, the loose arrangement of the spheroids exhibits low remolded shear strength.  
209 We suggest that the attraction-detachment model, based on the identification of  
210 mushroom-cap halloysite morphologies, provides a potential key for the identification of  
211 sensitive altered tephra that are predisposed to sudden failure that triggers landsliding.

212

### 213 **ACKNOWLEDGMENTS**

214 This research was funded by the DFG-Research Center MARUM (Bremen  
215 University) through INTERCOAST and University of Waikato. We thank C. Schulze for  
216 vane shear tests, B. Steinborn and C. Vogt for XRD analyses, P. Witte, A. Hübner, C.  
217 Schott, S. Buchheister, and V. Diekamp for laboratory assistance, M. Ikari, F. Sense, J.  
218 Lane, and P. Pasbakhsh for comments, and F. Terrible, J. K. Torrance, F. Cravero, M.  
219 McSaveney, and an anonymous reviewer for helpful reviews.

220

### 221 **REFERENCES CITED**

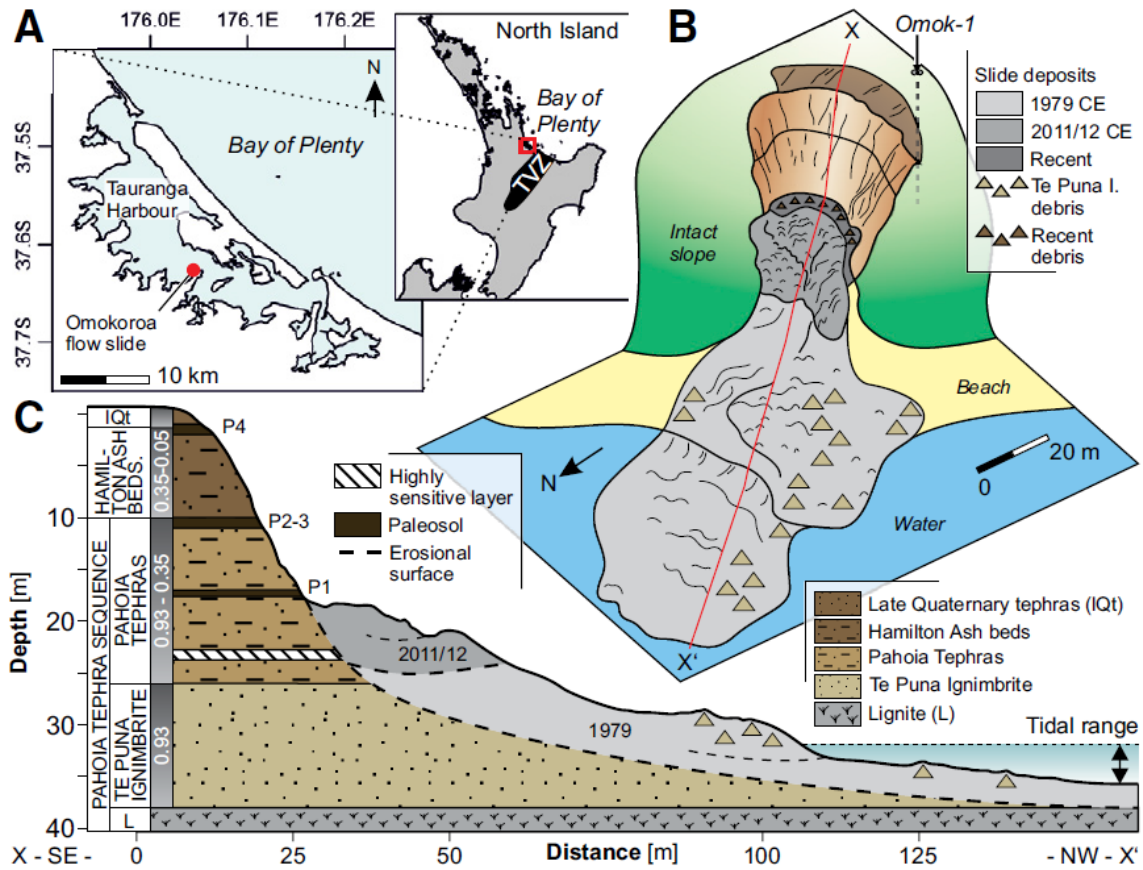
222 Berthonneau, J., Grauby, O., Jeannin, C., Chaudanson, D., Joussein, E., and Baronnet, A.,  
223 2015, Native morphology of hydrated spheroidal halloysite observed by  
224 environmental transmission electron microscopy: *Clays and Clay Minerals*, v. 63,  
225 p. 368–377, doi:10.1346/CCMN.2015.0630503.  
226 Briggs, R., Houghton, B., McWilliams, M., and Wilson, C., 2005,  $^{40}\text{Ar}/^{39}\text{Ar}$  ages of  
227 silicic volcanic rocks in the Tauranga-Kaimai area, New Zealand: dating the  
228 transition between volcanism in the Coromandel Arc and the Taupo Volcanic Zone:

- 229 New Zealand Journal of Geology and Geophysics, v. 48, p. 459–469,  
230 doi:10.1080/00288306.2005.9515126.
- 231 Chau, K., Sze, Y., Fung, M., Wong, W., Fong, E., and Chan, L., 2004, Landslide hazard  
232 analysis for Hong Kong using landslide inventory and GIS: Computers &  
233 Geosciences, v. 30, p. 429–443, doi:10.1016/j.cageo.2003.08.013.
- 234 Chigira, M., 2014, Geological and geomorphological features of deep-seated catastrophic  
235 landslides in tectonically active regions of Asia and implications for hazard mapping:  
236 Episodes, v. 37, p. 284–294.
- 237 Churchman, G.J., and Lowe, D.J., 2012, Alteration, formation, and occurrence of  
238 minerals in soils, *in* Huang, P. M., Li, Y., and Sumner, M. E., eds., Handbook of Soil  
239 Sciences: Properties and Processes (second edition): Boca Raton, Florida, CRC  
240 Press, p. 20.21–20.72.
- 241 Churchman, G.J., Pasbakhsh, P., Lowe, D.J., and Theng, B.K.G., 2016, Unique but  
242 diverse: some observations on the formation, structure, and morphology of  
243 halloysite: Clay Minerals, v. 51, p. 395–416, doi:10.1180/claymin.2016.051.3.16.
- 244 Cravero, F., Maiza, P., and Marfil, S., 2012, Halloysite in Argentinian deposits: origin  
245 and textural constraints: Clay Minerals, v. 47, p. 329–340,  
246 doi:10.1180/claymin.2012.047.3.04.
- 247 Cunningham, M. J., Lowe, D. J., Wyatt, J. B., Moon, V. G., and Jock Churchman, G.,  
248 2016, Discovery of halloysite books in altered silicic Quaternary tephros, northern  
249 New Zealand: Clay Minerals, v. 51, p. 351–372, doi:10.1180/claymin.2016.051.3.16.
- 250 Frolov, Y., and Maling, D., 1969, The accuracy of area measurement by point counting  
251 techniques: The Cartographic Journal, v. 6, p. 21–35, doi:10.1179/caj.1969.6.1.21.

- 252 Guimarães, L., Enyashin, A.N., Seifert, G., and Duarte, H.A., 2010, Structural, electronic,  
253 and mechanical properties of single-walled halloysite nanotube models: The Journal  
254 of Physical Chemistry C, v. 114, p. 11358–11363, doi:10.1021/jp100902e.
- 255 Israelachvili, J.N., 2011, Intermolecular and Surface Forces (3rd Edition): Waltham,  
256 Massachusetts, Academic Press, 704 p.
- 257 Jacquet, D., 1990, Sensitivity to remoulding of some volcanic ash soils in New Zealand:  
258 Engineering Geology, v. 28, p. 1–25, doi:10.1016/0013-7952(90)90031-U.
- 259 Joussein, E., Petit, S., Churchman, J., Theng, B., Righi, D., and Delvaux, B., 2005,  
260 Halloysite clay minerals—a review: Clay Minerals, v. 40, p. 383–426,  
261 doi:10.1180/0009855054040180.
- 262 Kirk, P., Campbell, S., Fletcher, C., and Merriman, R., 1997, The significance of primary  
263 volcanic fabrics and clay distribution in landslides in Hong Kong: Journal of the  
264 Geological Society, v. 154, p. 1009–1019, doi:10.1144/gsjgs.154.6.1009.
- 265 Kirkman, J.H., 1981, Morphology and structure of halloysite in New Zealand tephras:  
266 Clays and Clay Minerals, v. 29, p. 1–9, doi:10.1346/CCMN.1981.0290101.
- 267 Lowe, D.J., 2011, Tephrochronology and its application: a review: Quaternary  
268 Geochronology, v. 6, p. 107–153, doi:10.1016/j.quageo.2010.08.003.
- 269 Moon, V.G., 2016, Halloysite behaving badly: Geomechanics and slope behaviour of  
270 halloysite-rich soils: Clay Minerals, v. 51, p. 517–528,  
271 doi:10.1180/claymin.2016.051.3.09.
- 272 Moon, V.G., Lowe, D.J., Cunningham, M.J., Wyatt, J.B., de Lange, W.P., Churchman,  
273 G.J., Mörz, T., Kreiter, S., Kluger, M.O., and Jorat, M.E., 2015, Sensitive  
274 pyroclastic-derived halloysitic soils in northern New Zealand: interplay of  
275 microstructure, minerals, and geomechanics, in Rotonda, T. et al., eds., Volcanic

- 276 Rocks and Soils. Proceedings of the International Workshop on Volcanic Rocks and  
277 Soils, Lacco Ameno, Ischia Island, Italy: London, Taylor and Francis, p. 3–21.
- 278 Moon, V., 2016, Halloysite behaving badly: geomechanics and slope behaviour of  
279 halloysite-rich soils: *Clay Minerals*, v. 51, p. 517-528,  
280 doi:10.1180/claymin.2016.051.3.09.
- 281 Reed, S.J.B., 2005, *Electron Microprobe Analysis and Scanning Electron Microscopy in*  
282 *Geology*: Cambridge, UK, Cambridge University Press, 212 p,  
283 doi:10.1017/CBO9780511610561.
- 284 Rosenqvist, I.T., 1953, Considerations on the sensitivity of Norwegian quick-clays:  
285 *Geotechnique*, v. 3, p. 195–200, doi:10.1680/geot.1953.3.5.195.
- 286 Skempton, A., and Northey, R., 1952, The sensitivity of clays: *Geotechnique*, v. 3,  
287 p. 30–53, doi:10.1680/geot.1952.3.1.30.
- 288 Smalley, I., Ross, C.W., and Whitton, J., 1980, Clays from New Zealand support the  
289 inactive particle theory of soil sensitivity: *Nature*, v. 288, p. 576–577,  
290 doi:10.1038/288576a0.
- 291 Tanaka, K., 1992, Slope hazards and clay minerals: *Nendo Kagaku (Journal of the Clay*  
292 *Science Society of Japan)*, v. 32, p. 16–22.
- 293 Terzaghi, K., 1944, Ends and means in soil mechanics: *Engineering Journal*, v. 27,  
294 p. 608–615.
- 295 Vogt, C., Lauterjung, J., and Fischer, R.X., 2002, Investigation of the clay fraction (< 2  
296 µm) of the Clay Minerals Society reference clays: *Clays and Clay Minerals*, v. 50,  
297 p. 388–400, doi:10.1346/000986002760833765.
- 298 Wada, S.-I., Aoki, K., and Wada, K., 1977, The interior structure of spherical halloysite  
299 particles: *Clay Science*, v. 5, p. 113–121.

300



301

302

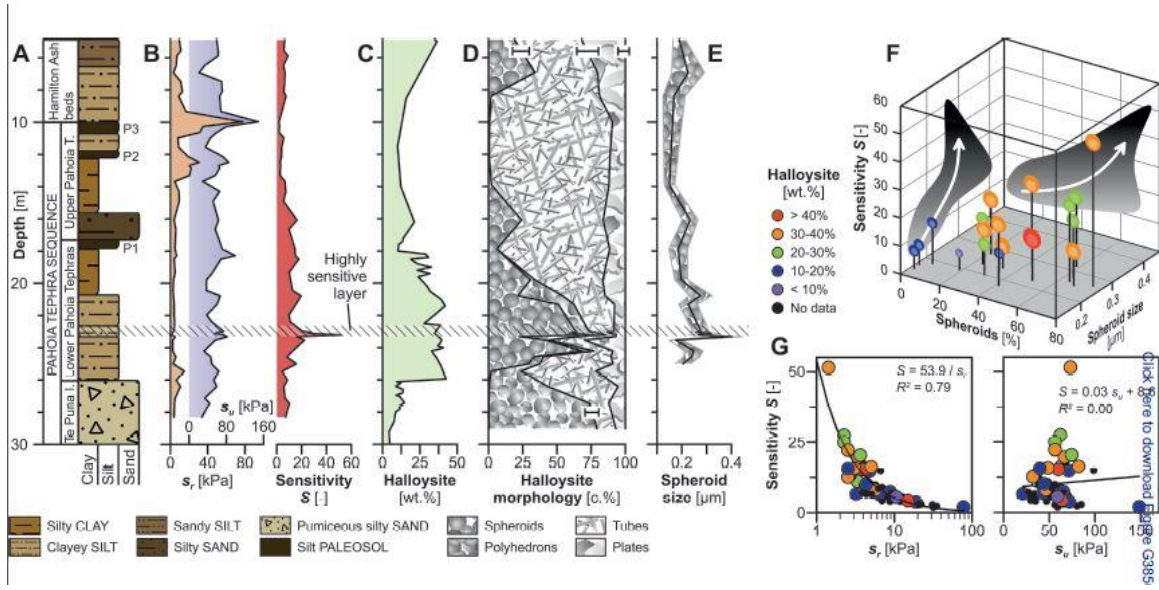
303 Figure 1. A: Map of Tauranga Harbour, New Zealand, with Taupo Volcanic Zone (TVZ)

304 as main source for Quaternary tephras at study site. B: Three-dimensional view of the

305 flow slide at Bramley Drive, Omokoroa; red line marks the position of profile in C. I.–

306 Ignimbrite. C: Profile through the flow slide with simplified stratigraphy and associated

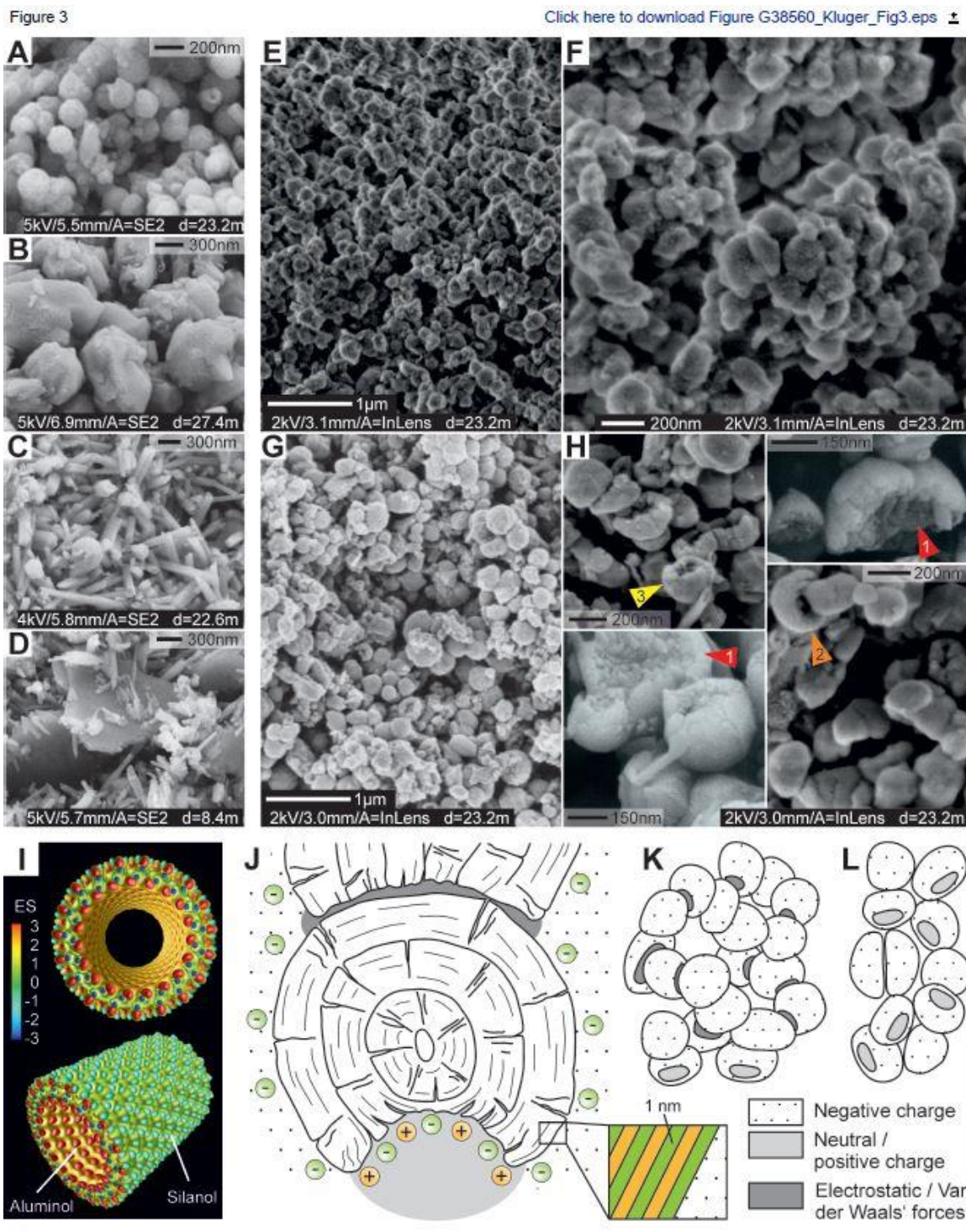
307 paleosols (P1–4) of core Omok-1 and ages (in Ma) after Moon et al. (2015).



308

309

310 Figure 2. A: Stratigraphy of core Omok-1 after Moon et al. (2015) showing main  
 311 lithological units as defined in Figure 1, three paleosols (P1–P3), and the highly sensitive  
 312 white layer at 23 m depth (hatched area). I.– Ignimbrite; T.– Tephtras. B: Undisturbed ( $s_u$ ,  
 313 blue) and remolded ( $s_r$ , orange) shear strength, and sensitivity ( $S = s_u/s_r$ ). C: Halloysite  
 314 bulk concentration. D: Cumulative volume percent (c. vol%) of halloysite morphologies  
 315 with bars indicating average standard deviations. E: Average spheroid sizes with standard  
 316 deviations depicted by fill patterns. F: Three-dimensional line plot illustrating  
 317 relationship between spheroid content, sensitivity, spheroid size, and halloysite  
 318 concentration; gray graded areas enable trends in sensitivity to be visualized. G:  
 319 Dependency between sensitivity and shear strength.



320

321 Figure 3. Scanning electron microscopy (SEM) images of spheroids (A), polyhedrons

322 (B), tubes (C), and plates (D) representing the main halloysite morphologies in Pahoia

323 Tephra sequence (New Zealand). E-H: SEM images from the highly sensitive layer of

324 undisturbed and multiply-connected halloysite spheroids (E, F) and remolded spheroids  
325 (G, H) showing smaller clusters or detached spheroids within much looser particle  
326 network. 1– exposed layers in spheroid openings; 2– partially separated halloysite  
327 spheroids; 3– detached mushroom cap–shaped halloysite spheroid. I: Electrostatic field  
328 proximal to halloysite nanotubes with colored equipotential surfaces (ES), modified with  
329 permission from Guimarães et al. (2010), copyright 2010 American Chemical Society. J:  
330 Conceptual mushroom cap–shaped spheroid cross-section and weak electrostatic and/or  
331 van der Waals attractions arising between exposed silanol-aluminol sheets in spheroid  
332 openings and the negatively-charged convex exterior surfaces; enlargement is adapted  
333 from Berthonneau et al. (2015). Circles with + and – relate to the positive and negative  
334 electrostatic field proximal to the spheroid’s exterior surface. Mushroom cap–shaped  
335 spheroids connect with one another between concave openings and convex outer spheroid  
336 surfaces, forming aggregates (K) which are partly detached because of remolding (L).